How can existing ground-based profiling instruments improve European weather forecasts?

Article

Accepted Version

Illingworth, A. J. ORCID: https://orcid.org/0000-0002-5774-8410, Cimini, D., Haefele, A., Haeffelin, M., Hervo, M., Kotthaus, S., Löhnert, U., Martinet, P., Mattis, I., O'Connor, E. J. and Potthast, R. (2019) How can existing ground-based profiling instruments improve European weather forecasts? Bulletin of the American Meteorological Society. pp. 605-619. ISSN 0003-0007 doi: 10.1175/BAMS-D-17-0231.1 Available at https://centaur.reading.ac.uk/82250/

The DOI for this manuscript is doi: 10.1175/BAMS-D-17-0231.1

Illingworth, A., D. Cimini, A. Haefele, M. Haeffelin, M. Hervo, S. Kotthaus, U. Löhnert, P. Martinet, I. Mattis, E. O'Connor, and R. Potthast, 2018: How can Existing Ground-Based Profiling Instruments Improve European Weather Forecasts?. Bull. Amer. Meteor. Soc. doi:10.1175/BAMS-D-17-0231.1, in press.

How can Existing Ground-Based Profiling Instruments Improve European Weather Forecasts?

Authors:

A. J. Illingworth[*1], D. Cimini[2], A. Haefele[3], M. Haeffelin[4], M. Hervo[3], S. Kotthaus[4], U. Löhnert[5], P. Martinet[6], I. Mattis[7], E. J. O'Connor[8], and R. Potthast[9]

Affiliations:

[1]Department of Meteorology, University of Reading, UK

[2]CNR-IMAA, Potenza, Italy & CETEMPS, University of L'Aquila, Italy

[3]MeteoSwiss, Payerne, Switzerland

[4]Institut Pierre Simon Laplace, Ecole Polytechnique, Palaiseau, France

[5]Institute for Geophysics and Meteorology, University of Cologne, Germany

[6]CNRM UMR 3589, Meteo France/CNRS, Toulouse, France

[7]Deutscher Wetterdienst, Observatorium Hohenpeißenberg, Germany

[8]Finnish Meteorological Institute, Finland

[9]Deutscher Wetterdienst, Offenbach, Germany

* *Corresponding author address*: Anthony J. Illingworth, Department of Meteorology, University of Reading, Earley Gate, PO Box 243, Reading RG6 6BB, UK

Tel: +44 118 378 6508 E-mail: a.j.illingworth@reading.ac.uk

ABSTRACT

To realise the promise of improved predictions of hazardous weather such as flash floods, wind storms, fog and poor air quality from high-resolution mesoscale models, the forecast models

must be initialized with an accurate representation of the current state of the atmosphere, but the lowest few km are hardly accessible by satellite, especially in dynamically-active conditions. We report on recent European developments in the exploitation of existing ground-based profiling instruments so that they are networked and able to send data in real-time to forecast centers. The three classes of instruments are: (i) Automatic lidars and ceilometers providing backscatter profiles of clouds, aerosols, dust, fog and volcanic ash, the last two being especially important for air traffic control; (ii) Doppler wind lidars deriving profiles of wind, turbulence, wind shear, wind-gusts and low-level jets; and (iii) Microwave radiometers estimating profiles of temperature and humidity in nearly all weather conditions. Twenty-two European countries and fifteen European National Weather Services are collaborating in the project, that involves the implementation of common operating procedures, instrument calibrations, data formats and retrieval algorithms. Currently, data from 220 ceilometers in 17 countries are being distributed in near real-time to national weather forecast centers; this should soon rise to many hundreds. The wind lidars should start delivering real time data in late 2018, and the plan is to incorporate the microwave radiometers in 2019. Initial data assimilation tests indicate a positive impact of the new data.

CAPSULE

Observations of profiles of winds, aerosol, clouds, winds, temperature and humidity in the lowest few km of the atmosphere from networks of ceilometers, Doppler wind lidars and microwave radiometers are starting to flow in real time to forecasting centers in Europe.

The high-resolution (1 km) forecasting models that are now run operationally by many European National Weather Services promise to provide increasingly accurate high-resolution forecasts of impending hazardous weather, ranging from flash floods to episodes of poor air

quality. The WMO guidance for NWP applications highlights the need for wind, temperature and humidity profiles, especially in cloudy areas[1]. Satellites can provide data in the upper troposphere, but if this promise is to be fulfilled, in particular for short-range forecasts, a new generation of high-density observations through the lower few km of the atmosphere, including the boundary layer, is required in real-time. This region close to the ground is particularly difficult to observe with satellites due to the frequent occurrence of clouds and, for passive instruments, the broad weighting functions and the effects of the variable albedo or brightness temperature of the surface.

Illingworth et al. (2015) noted the potential of ground-based networks of automatic low-power backscatter lidars/ceilometers (ALC)[2], Doppler Wind Lidars (DWL) and Microwave Radiometers (MWR) to supply real-time observation to forecast centers. In this paper we report recent developments in the exploitation of these networks. Observations of profiles of aerosols, clouds, winds, temperature and humidity in the lowest few km of the atmosphere in Europe are now starting to flow in real time to forecasting centers. This has been achieved as a result of collaboration between a COST action (see sidebar) 'TOPROF: Towards operational ground-based profiling with ALCs, DWL and MWRs for improving weather forecasts' (www.cost.eu/COST_Actions/essem/ES1303) and EUMETNET, an organization which provides a framework to enable the European Weather Services to work together, share ideas, best practice and to share the cost of major infrastructure investments. The EUMETNET Composite Observing System (EUCOS) is responsible for developing an observing system for

[1] See WMO statements of guidance for high-resolution and global NWP at:
https://www.wmo.int/pages/prog/www/OSY/SOG/SoG-HighRes-NWP.pdf
https://www.wmo.int/pages/prog/www/OSY/SOG/SoG-Global-NWP.pdf

[2] Ceilometers were originally conceived to measure cloud base altitude only, but today the sensitivity of these instruments is sufficient to provide profiles of backscattered power from aerosols and clouds. Hence a new terminology has been proposed that combines automatic low-power lidars and ceilometers into ALCs.

Europe serving the needs of regional numerical weather prediction (NWP). One of EUMETNET's programs is 'E-PROFILE' that originally involved only radar wind profilers, but has been extended to include ALC networks and more recently is incorporating DWLs with a projected extension to distribute MWR data. The TOPROF action ran from October 2013 to October 2017 with financial support from the European Union and was responsible for setting up common calibration techniques, operating procedures, deriving error characteristics, developing retrieval algorithms, and ensuring homogeneous and reliable data quality for the three classes of instruments, whereas EUMETNET through its E-PROFILE program is involved in the networking and near real-time distribution of observations to the national weather services.

The ALCs under investigation in the E-PROFILE network transmit short pulses of laser radiation with wavelengths 532, ~ 910 or 1064 nm and receive a backscattered signal with a delay that provides range information. The raw data are averaged to 15-30m vertical resolution and 15-60 seconds in time. Examples of the use of attenuated backscatter profiles include characterising clouds, aerosols, dust, fog and volcanic ash as discussed in more detail in the ALC section, the last two being especially important for air traffic control. At present, attenuated backscatter profiles from over 220 ALCs in 17 countries are being distributed by EUMETNET E-PROFILE in near real-time to National Weather Services and can be viewed at http://eumetnet.eu/e-profile/, (Wiegner et al. 2014). These data are homogenized and calibrated using the developments carried out in TOPROF.

Fig. 1 represents the map of E-PROFILE stations in green and stations that will be integrated before the end of 2018 in blue: ALCs that are present in Europe but not yet integrated into E-PROFILE are in red (data from DWDs ceilomap https://www.dwd.de/ceilomap). In June 2018,

the Saddleworth Moor fire near Manchester injected large quantities of smoke into the atmosphere. This smoke was transported over UK and Europe and measured by the E-PROFILE network. The measurements from 26 to 28 June at five E-PROFILE stations are displayed in Fig. 1. Aerosol layers are visible in the free troposphere (at altitudes between 2 and 5 km). Measurements above thick clouds (represented with black dots) appear as white vertical stripes because the laser beam is fully attenuated. These measurements are also visible on the E-PROFILE website and clearly illustrate the capabilities of the network in monitoring aerosol layers over Europe.

In contrast to ALCs which have been in use for many years, DWLs have undergone recent development using solid-state fibre-optic technology at a wavelength of ~1.5 μm. The type of DWL being incorporated into the E-PROFILE network obtains the radial Doppler shift of the backscattered signal from aerosol or cloud particles in the direction of the beam using the high pulse rate heterodyne technique. From the radial Doppler velocities, the vertical structure of winds, wind shear, levels of turbulence, inference of the maximum gusts, properties of low-level jets and classification of the state of the boundary layer can be obtained. The minimum range is typically 50-90 m, with the maximum range varying from 2-10 km; in practice the sensitivity of most instruments usually limits the observations to within the boundary layer where there are sufficient aerosols. Wind measurements are not possible inside or above optically thick clouds or in heavy rain.

Ground-based microwave radiometers (MWR) measure the natural down-welling thermal emission in the microwave part of the electromagnetic spectrum originating from Earth's atmosphere and the cosmic background. The radiance observations are commonly expressed as an equivalent brightness temperature (T_B) from which estimates of atmospheric temperature

profiles (from oxygen absorption from 55 to 60 GHz) and humidity profiles (from water vapor absorption around 22 GHz) as well as column-integrated water vapor (IWV) and liquid water path (LWP) can be inferred during non-precipitating conditions. Valid temperature profiles can also be inferred in the presence of low-moderate precipitation. The MWR profiling capability in the lowest 2 km of the atmosphere is proving to be valuable because of the poor sampling by other sensors (e.g. from satellite).

All these instruments are rugged and can operate autonomously for long periods requiring little maintenance and do not need specialised staff, but how can these new observations contribute to NWP? Firstly, they can be used to check that the parameterisation schemes inherent in such models lead to a realistic representation of the current state of the atmosphere. For more than ten years the Cloudnet project (Illingworth et al. 2007) has used vertically pointing cloud radars, ACLs and MWRs to derive cloud properties, compared them with the representation of clouds within several operational European forecast models and produced statistics of the model performance (http://cloudnet.fmi.fi). In Cloudnet the ALCs were only used to identify cloud base of liquid clouds and the MWRs to derive their liquid water path. A more rigorous approach is to compare the observations ('O') with their representation in the model (the background 'B') to obtain the 'O-B' statistics and to check that any biases are sufficiently small and, ideally, that the errors are Gaussian. This procedure is fairly straightforward for the winds from a DWL because the model has a prognostic wind variable. This is not the case for the ALC backscatter signal nor for the brightness temperature from microwave radiometers, so a *'forward model'* must be used that operates on the prognostic variables within the NWP model to predict the value of the observed parameter which can then be directly compared with the observation. Once the O-B statistics are deemed to be acceptable then there is potential for *data assimilation* whereby the initial state of the model is updated with the observations

accounting for the errors in both the observations and the model, so that the NWP model can be initialised with the best possible representation of the current state of the atmosphere. A more accurate initial state usually reduces the errors in the forecast.

If the new observations are to be useful, then it is essential that the data are calibrated and unbiased and the quality is homogeneous with known error characteristics. TOPROF's major tasks have been to establish common calibration procedures for the three classes of instruments, common checks on data quality, and independent validation of the veracity of the data. TOPROF has also developed forward models for predicting the ALC and MWR observations from the NWP representation, and defined common data formats and protocols for transmitting the data to a central hub from where they can be distributed to the national weather services. Finally, TOPROF has started gathering O-B statistics of model performance and carried out some simple data assimilation trials that indicate a positive impact on the forecast.

AUTOMATIC LOW-POWER LIDARS AND CEILOMETERS (ALCS).

Figure 2 shows a warm front crossing Germany in the morning of 25 August 2018 as observed at Ulm by a CHM15-k ceilometer of the DWD network. The cloud base height descended from 10 km at midnight to 2.5 km at 0800 UTC. Rain started at 0900 UTC, visible as red vertical stripes between the cloud base and the ground. The yellowish horizontal line at 2 km altitude between 1200 and 1500 UTC shows the melting layer (dark band). After the frontal passage (at about 1500 UTC), the steady rain stopped and the stratiform clouds were replaced by broken cumulus, with some precipitation below cloud base that occasionally reached the ground. Liquid water clouds can be identified by a thin layer with very high backscatter at cloud base followed by rapid extinction of the ceilometer signal, for example near heights of 2-3 km at 0000, 0200 and from 1700 - 2100 UTC, whereas the ceilometer signal penetrates further into

ice clouds. Before the frontal passage the planetary boundary layer (PBL) was characterized by a significant aerosol load with backscatter values > 1 Mm^{-1} sr^{-1} up to ~2 km height, but was cleaner during the afternoon; this could be due to wash-out or a different, cleaner air mass. Note the two thin aerosol layers from long range transport (in yellow) at 8 and 10.5 km altitude after 2200 UTC with backscatter values ~ 0.5 Mm^{-1} sr^{-1}, possibly from forest fires in North America.

Three classes of ALCs are being used in the E-PROFILE network. CL31 and CL51 from Vaisala measuring at ~ 910 nm, CHM15k from Lufft measuring at 1064 nm and Mini-MPL from Sigma-Space, measuring at 532 nm. Other ALCs are also exploited at some sites such as, for example, the CS135 from Campbell Scientific (910 nm) or the CE370 from CIMEL (532 nm). ALCs are characterized by their continuous 24-7 operation capabilities with high sampling rates. In the low-altitude range, the optical overlap between the emitting (laser) and receiving (telescope) optical components of an ALC changes with altitude. If this overlap function is not well characterized, exploitation of the measurements at low-altitude may be restricted. In the far-altitude range, the signal-to-noise ratio may limit the exploitation of the measurements for detecting low-scattering media such as aerosols. Some more sensitive systems may, on the contrary, suffer from saturation due to high-scattering media such as liquid water clouds at short range. Some of these effects can be corrected to improve signal quality. All ALCs must also be calibrated in order to derive quantitatively meaningful attenuated backscatter profiles that can be compared from one instrument to the next and with values predicted from NWP forward models.

a*) Determining optical overlap functions.* The optical design of CL31 (CL51) instruments yield a complete overlap around 50m (200m) (e.g. Haeffelin et al. 2012; Wiegner et al. 2014). The bi-axial lidars like CHM15k or Mini-MPL reach complete optical overlap around 1km with

very noisy signal below 150-200 m, a region where the optical overlap is close to zero. Hervo et al. (2016) found that the optical overlap function of the CHM15k is affected by temperature fluctuations. They developed a methodology to determine the temperature dependence and correct for it, yielding a precise attenuated backscatter values in the partial overlap region.

b) *Correcting signal artifacts*. Kotthaus et al. (2016) found signal artifacts in the free troposphere in CL31 attenuated backscatter profiles, characterized by negative values in cloud-free regions due to a shift of the raw data introduced by the system firmware, and developed a method to quantify these artifacts and correct for them. These results convinced Vaisala to release a new firmware for TOPROF that removes the artificial shifts to allow more quantitative exploitation of the CL31 attenuated backscatter profiles;

c) *ALC Calibration*. The signal detected by the ceilometers must be converted into an absolute value of backscatter measured in units of m^{-1} sr^{-1}. This is best accomplished by using a reference target whose backscatter characteristics are known. One approach uses the known integrated backscatter for a water cloud that total extinguishes the ceilometer signal; this can be obtained by adding the observed backscatter at each gate within the cloud, and adjusting the ceilometer calibration until this integral, after correction for multiple scattering, is equal to 0.027 m^{-1}. For details see O'Connor et al. (2004). Hopkins et al. (submitted to AMT) showed that this calibration is accurate to better than 10% with no significant annual variation. A second approach for photon-counting instruments measuring at 532 or, more commonly at 1064 nm, is to use the molecular return as a reference because it is a function of the known air density (Fernald et al. 1972; Klett, 1985; Wiegner and Geiß, 2012; Baars et al. 2016). The molecular return at 1064 nm is small, but photon counting instruments are able to measure it with sufficiently long averaging times (Wiegner and Geiß, 2012) and Fig. A2 in Baars et al. (2016). The method developed within TOPROF relies on averaging the backscatter return for 6 hours on a clear night; sensitivity studies showed that typical accuracies of the calibration are

of the order of 10%-15%. The calibrations can be up to a factor of two different from those supplied by the manufacturer. These two methods are implemented by E-PROFILE to distribute calibrated attenuated backscatter data to national weather services. Wiegner and Gasteiger (2015) propose a method to correct for water vapor absorption for ALC measurements that operate at wavelengths affected by this effect (e.g. 905-910 nm).

d) *ALC measurement uncertainties for Lufft and Vaisala due to incomplete optical overlap, signal artifacts, and calibration*. These have been estimated using data from a three-month experiment 'CEILINEX' when 12 ALCs were operated side-by-side (https://ceilinex2015.de/, Pattantyús-Ábrahám et al. 2017). Fig. 3 shows a comparison of raw ALC signal and calibrated attenuated backscatter signal from 8 co-located ALCs including Campbell Scientific, Vaisala, and Lufft instruments based on 3 hours of data on 13 Aug 2015. The profiles show a stable nocturnal boundary layer up to 300 m and a residual layer up to 750 m. Additionally, there are two lofted aerosol layers (probably Saharan dust) between 1 and 4 km. Fig. 3 shows that differences less than 25% can be expected for calibrated attenuated backscatter, in particular for altitudes greater than 500 m. Below 500 m the greater differences between the Lufft and Vaisala instruments can be attributed to systematic errors in the overlap function correction. Note also inconsistencies below 250 m between CL31 and CL51 profiles and between the different Lufft ALCs, confirming that data should be used with great care at such low altitudes. CL31 and CL51 measurements have a lower signal-to-noise ratio than the other instruments at altitudes greater than 1000 m and so are less sensitive for monitoring lofted aerosol.

Applications using ALC measurements are numerous. Several studies were conducted in the framework of the TOPROF action that resulted in the evaluation of aerosols in atmospheric models based on ALC forward models and O-B statistics (e.g. Warren et al. 2018), providing diagnostics of the atmospheric boundary layer height (Lotteraner and Piringer 2016; Poltera et

al. 2017; Kotthaus and Grimmond, 2018), supporting warning of fog formation (Haaeffelin et al. 2016), and detecting transport of dust, biomass burning and volcanic ash (Cazorla et al. 2017; Roman et al. 2018). Fig. 4 shows an example of comparisons between attenuated backscatter observed by an ALC and modeled using the ECMWF CAMS forward model[3]. The observations were performed by a CHM15k in Valladolid and calibrated using the methodology described above. Saharan dust aerosols are clearly visible up to 5 km, both in the observations and the forecasts. The mean bias for this event is lower than 5%, showing the good agreement between observations and forecasts. Chan et al. (2018) carried out a year- long comparison of the representation of aerosols within the CAMS model and from the German ceilometer network and found very good agreement with the arrival time and vertical extent of a Saharan dust layer. Fig. 5 shows an example of low-altitude ALC-derived information during 3 hours in pre-fog conditions at the Charles-de-Gaulle airport near Paris. The bottom panel shows the 0-400 m ALC attenuated backscatter profile, while the top panel provides fog alerts based on Haeffelin et al. (2016). At 0430h, more than 1 hour before the first alerts, the sky is cloud free (bottom panel) favoring radiative cooling and the ALC backscatter is quite high between 50-150 m, revealing the presence of large aerosols in a moist atmosphere. At 0550h, a cloud forms about 100 m agl generating severe-level alerts aloft, and rapidly subsides to the ground, leading to persistent fog after 0645h, about 1 hour after the first severe-level alerts.

DOPPLER WIND LIDARS (DWLs)

The Doppler lidar instruments considered by the TOPROF action were those with sufficient sensitivity and a scanning capability so that the horizontal wind profile could be derived throughout the boundary layer. These included instruments from Halo Photonics (Streamline,

[3] Developed for the CALIOP lidar data from CALIPSO satellite in the A-train, (Benedetti et al., 2009) but looking upwards instead of downwards. The model carries aerosol type and size and so the optical depth/extinction is calculated, and the assumed lidar ratio converts extinction into the observed value of backscatter.

Streamline Pro and Streamline XR) and Leosphere (WindCube 100S, 200S and 400S), all configurable to have a maximum range of about 10 km and range resolution of 50 m or better. All DWL considered in TOPROF are full-hemispheric scanning, except for the Halo Photonics Streamline Pro, which can scan within a cone from 70° above the horizon to zenith and has no external moving parts. One task in TOPROF was to design suitable scanning strategies optimized to extract as much information as possible. The scanning capability is utilized to reconstruct the vertical profile of the horizontal wind from the measured radial components. This can be performed in a similar manner as for radar wind profilers by means of 'Doppler Beam Swinging' where the wind speed and direction are derived from the radial (line-of-sight) components from off-zenith dwells at different azimuths, or by using a conical Velocity-Azimuth-Display (VAD) scan where the wind speed and direction can be inferred from the magnitude and phase of the sinusoidal azimuthal variation of the observed radial component of the wind. Both methods rely on assuming horizontal homogeneity in order to derive the horizontal component; this may not be applicable in strongly turbulent situations, or in flows over complex terrain. TOPROF recommends performing a VAD scan with a minimum of 12 beams, and, using the method of Päschke et al. (2015), which, in addition to generating the horizontal wind profile, provides a metric describing the likelihood of inhomogeneity degrading the retrieval. Teschke and Lehmann (2017) note that the optimal elevation angle for a VAD scan is about 35° from horizontal but that this is not a strong constraint; suitable elevation angles for VAD scanning lie between 15 and 70° from horizontal. Hence, TOPOROF recommends performing two VAD scans; a primary scan at high elevation (50-70° from horizontal) to capture the wind profile to the top of the boundary layer; and a rapid low-elevation scan at 15° or lower in elevation (dependent on local obstructions), from which the vertical profile can be extended down towards the surface below the minimum altitude probed by the higher elevation scan. The inclusion of an additional scan at a low elevation can also be

used to investigate the spatial representativeness of the wind profile.

Such high vertical resolution wind profiles are ideal for capturing the presence of wind shear, and low-level jets, an important consideration for wind energy, aviation, and air quality applications. An objective method for diagnosing low-level jets was developed (Tuononen et al., 2017) and is now being implemented routinely at a number of sites (Marke et al., 2018). Vertical dwells with high temporal resolution (5 seconds or better) within the VAD scans allow the retrieval of turbulent parameters such as vertical velocity variance, skewness and dissipation rate of turbulent kinetic energy (O'Connor et al., 2010). Combining these parameters permits a classification of the atmospheric boundary layer structure (Manninen et al, 2018) in which the turbulent regions are detected, and a probable source of turbulence assigned: e.g. whether wind shear or buoyancy production dominates, or whether convection is surface-driven or cloud-driven. The classification scheme also notes whether the turbulent layers are in contact with the surface, an important distinction when calculating dispersion in chemical transport models. Turbulent parameters can also be derived from VAD scans (Vakkari et al., 2015), reconstructed using a stochastic particle filter (Rottner et al., 2017), and the combination of winds and turbulence can be used to diagnose wind gusts (Suomi et al., 2017) especially important in forecasting and assessing wind-induced damage.

DWL products can be used to validate the boundary layer schemes employed in forecast models, even in challenging locations (a coastal example is given in Fig. 6), and to evaluate the much more spatially dense ALC retrievals (Schween et al. 2014). Generating these new products routinely requires that DWL uncertainties are known and well characterized. Known hard targets such as towers and masts can be used to check the radial Doppler velocity, and that the pointing angle is correct. Azimuthal pointing repeatability for these instruments was shown

to be excellent, typically within 0.25°. Uncertainties in radial Doppler velocity estimates are a function of the number of pulses sampled and their signal-to-noise ratio (SNR). TOPROF worked together with the manufacturers on understanding and improving the data processing to yield reliable data. Reducing the median bias in SNR to about 0.0002 led to improvements in sensitivity by as much as a factor of 5 to 10 (Manninen et al. 2016), so that a lower SNR threshold could be used to diagnose 'good' data. The bias reduction permits more reliable uncertainty estimates, yielding more accurate turbulent parameters. Long-term comparisons of the resulting wind estimates compare very well with masts and other measurements at high SNR with root mean squared errors, RMSE, of < 0.7 m s^{-1} for wind speed and $< 10°$ for direction (e.g. Päschke et al. 2015), but care should be taken when calculating wind climatologies in low SNR conditions (Gryning et al. 2016). Now that the data quality has been established the next step is a to establish the O-B statistics. In principle, DWLs provide profiles of attenuated backscatter similar to ALCs. DWLs operating with a telescope focused at infinity can use the same liquid cloud method as for ALCs (Westbrook et al. 2010) for calibrating the backscatter power. However, by adjusting the telescope focus, extra sensitivity in the BL can be achieved while sacrificing sensitivity in the far range; beneficial for retrieving winds and turbulence in the boundary layer, but more difficult to account for in calculating the profile of attenuated backscatter. Extensive comparisons with instrumented towers confirm the accuracy of the winds derived from DWLs and a more comprehensive O-B comparison is planned using the two-year data set obtained from the DWL network.

MICROWAVE RADIOMETERS (MWRs)

MWR measure downwelling radiation in terms of atmospheric brightness temperatures (T_B) that are then converted to atmospheric variables of interest. TOPROF fostered breakthrough

345 developments in both MWR hardware and software leading to more accurate T_B observations,
346 relevant for direct data assimilation, and also to improved retrievals of atmospheric variables.
347 The instruments considered here are multi-channel temperature and humidity profilers
348 operating in the 22-31 (humidity) and 51-60 (temperature) GHz bands, such as Radiometer
349 Physics (RPG)[4] HATPRO and Radiometrics MP3000[5] (Ware et al. 2003; Rose et al. 2005; De
350 Angelis et al. 2017). These instruments also provide the column-integrated amount of water
351 vapor (IWV) and cloud liquid water path (LWP).
352
353 Two Joint Calibration (JCAL) field experiments were organized in cooperation with leading
354 MWR manufacturers, triggering the development of new calibration targets and receiver
355 technology. RPG has developed a new arrangement for the liquid nitrogen calibration target
356 that eliminates calibration uncertainties due to reflections and standing waves and provides
357 absolute accuracies of T_B on the order of 0.1 K, which is a factor ~5 more accurate than
358 previous targets. The load was introduced with the 5th HATPRO generation, which also
359 includes an improved receiver technology resulting in T_B noise levels also on the order of 0.1
360 K at 1 s temporal resolution. Czekala (personal communication) has shown that this can lead
361 to an uncertainty reduction of the temperature profile retrieval by up to 0.3 K, leading to more
362 reliable detection of temperature inversions in the boundary layer. These hardware
363 developments can also improve the accuracy of IWV and LWP retrievals by up to 50%. The
364 new calibration load is also compatible with radiometers of older generations.
365 Recommendations for operational calibration, measurement and quality procedures suited for
366 network operation were agreed upon and distributed
367 (http://cetemps.aquila.infn.it/mwrnet/reports.html). In addition, a software package for data

[4]https://www.radiometer-physics.de/products/microwave-remote-sensing-instruments/radiometers/humidity-and-temperature-profilers/
[5]http://radiometrics.com/mp-series/

post-processing including retrieval application, quick-look generation, and output conversion (compliant with the Climate and Forecast metadata convention) for most common MWR types is available (http://cetemps.aquila.infn.it/mwrnet/mwr_pro.html).

A fast forward model has been developed (De Angelis et al. 2016) by adapting existing software widely used for satellite data assimilation so that it can calculate the downwelling T_Bs that would be observed at the ground and their Jacobians from any source of atmospheric temperature and humidity profiles (e.g. radiosondes or an NWP model). The software, RTTOV-gb, (http://cetemps.aquila.infn.it/mwrnet/rttovgb.html), is freely available, and validation with a reference line-by-line (LBL) computation shows unbiased rms differences within 0.2 K, so the error of the parametrized forward model is within the instrumental uncertainty. In order to monitor the behavior of continuous T_B observations, O-B statistics were computed for a 1-year dataset from a prototype network of six MWRs (De Angelis et al. 2017). Within this network standardized calibrations procedures and data life cycle had been implemented so that quality-controlled data were collected. The six prototype network stations are located at: Cabauw, NL (51.97N/4.93E), Jülich, GER (50.91N/6.41E), Leipzig, GER (51.35N/12.43E), Lindenberg, GER (52.21N/14.12E), Palaiseau, FRA (48.40N/2.36E), and Payerne, SUI (46.82N/6.95E). Fig. 7 shows the 1-year time series of O-B comparison at one site for four frequency channels. The NWP model used here is AROME, Application of Research to Operations at Mesoscale, developed by Météo-France (Seity et al. 2011).

The O-B analysis revealed that typical differences are within the expected total uncertainty and that the O-B distributions were Gaussian, confirming their suitability for variational data assimilation. The analysis also demonstrated how such monitoring is able to detect an instrument malfunction leading to a mis-calibration and then to verify that a re-calibration has

been successful as described in Fig. 7. The O-B analysis showed consistent characteristics over time and instrument site/type with a typical O-B bias for well-maintained instruments being generally below 1K, but reaching ~3K at lower frequency oxygen channels, where the forward model uncertainty reaches its maximum (De Angelis et al. 2017; Cimini et al. 2018). However, even these uncertainties can be effectively addressed because the biases were persistent and the random component was similar throughout the prototype network. The uncertainty of the reference LBL calculations have also been investigated (Cimini et al. 2018), possibly explaining systematic O-B differences exceeding 1 K that must be accounted for within a bias correction scheme. A platform for continuously monitoring O-B quick-looks in near-real-time is up and running and available for all interested users (https://tinyurl.com/MWR-O-B-JOYCE). The main goal of this platform is i) to provide an independent instrument performance monitoring tool for MWR operators and ii) to attest the suitability of MWR for operational use by National Weather Services.

In addition to the prototype network, there are some 30 MWR stations over Europe that have the potential to deliver T_Bs and derived products on a continuous basis. Details of the network can be found at http://cetemps.aquila.infn.it/mwrnet/MWRnetmap.html. Long data records (exceeding 10 years) are available from some of these sites, in Europe (e.g. Lindenberg (GER), Payerne (SUI), and Potenza (IT)) as well as in the USA (e.g. ARM sites; Cadeddu et al. 2013). MWR data assimilation promises to be useful for adjusting NWP model temperature and humidity fields of the lowest 2 km, especially in convective (Cimini et al. 2015) and very stable conditions (Martinet et al. 2017). Fig. 8 shows how the assimilation of MWR brightness temperatures leads to an improvement in the temperature analysis in an enclosed Alpine valley during stable conditions where the true structure has been established from a series of radiosonde ascents; the stability close to the ground is a crucial parameter in the build-up and

dispersion of pollutants. Similarly, Fig. 9 shows large potential improvements in both temperature and humidity profiles when observations from one MWR are used to correct the NWP forecast, in a so-called one-dimensional variational retrieval (1DVAR) scheme. 24-hour time series of temperature and humidity profiles from a NWP forecast, 1DVAR retrievals, and the analysis increment are shown. Based on these results, Météo-France decided to deploy a MWR network for an international fog field campaign planned for Dec 2019-Feb 2020 (four to six MWR units in a 300x200 km domain). Forecast indices derived from MWR observations were also demonstrated to be useful in support of nowcasting and short-range weather forecasting (Cimini et al. 2015). Continental-scale data assimilation trials show positive-to-neutral impact, especially for accumulations of precipitation up to 18h after forecast initialization (Caumont et al. 2016). The impact of MWR-derived thermodynamic profiles is larger when they are used to substitute classical radiosonde observations in a data denial experiment. Data assimilation results obtained so far did not take advantage of the recent hardware and software developments, so there is clearly potential for improvement.

CONCLUSIONS

Networks of ground-based profiling instruments with improved retrieval algorithms and standardized software and calibration procedures have been developed by TOPROF in collaboration with instrument manufacturers and implemented by the E-PROFILE program of the EUMETNET consortium of European National Weather Services. These networks are providing an increased understanding of process within the lowest few km of the atmosphere, and, ultimately, have the potential for assimilation into operational NWP models. Improvements have been made in the Automatic Lidar and Ceilometer (ALC) algorithms that correct for overlap, remove artifacts in the profiles, and provide absolute backscatter calibration to within ~10% using natural targets as a reference; either the integrated backscatter from thick

water clouds or the molecular return. The network has the demonstrated capability for tracking smoke from forest fires and desert dust, issuing fog formation warnings, and for providing vertical profiles of cloud and aerosols. An O-B comparison of the observed backscatter from desert dust with those from an ECMWF forward model indicates that biases are below 10%. Profiles of aerosol and cloud backscatter from a network of 220 ALCs (as of September 2018) are being distributed in real time to European weather forecast centers and this should increase to several hundreds within the next year.

A network of Doppler Wind Lidars (DWLs) is being set up and test data are now being distributed in experimental mode to forecast centers by E-PROFILE. DWLs use aerosol or cloud particles as tracers of the line of sight component of atmospheric motion. Standardized scanning procedures and algorithms have been established so they can routinely provide data on wind profiles in the boundary layer with an rms accuracy of $< 10°$ in direction and better than 0.7 m s^{-1} in speed. These observations can be used for diagnosis of the existence of low-level jets, deriving profiles of vertical velocity variance and skewness, and the dissipation rate of turbulent kinetic energy. The combination of the wind and turbulence can be used to diagnose wind gusts, needed for forecasting and assessing wind-induced damage, and for classification of the atmospheric boundary layer structure so that those turbulent layers in contact with the surface can be identified; this is an important property when calculating the dispersion by chemical transport models.

TOPROF studies have led to advances in Microwave Radiometer (MWR) hardware and software so the instruments can provide brightness temperature (T_B) calibrations to within 0.1K. A ground-based version of the RTTOV radiative transport model has been developed and characterized, so that T_B and its uncertainty can be calculated from a forecast model. Tests

over one year comparing these forward modeled values of T_B with those observed with a prototype network of six MWRs show that typical O-B biases for well-maintained instruments are generally below 1K. Field campaigns have demonstrated that the assimilation of T_B into an operational mesoscale model leads to improved temperature and humidity structure in the lowest 2 km of the atmosphere. E-PROFILE is evaluating the extension of their activities to MWR so that data can be distributed in real time to European weather forecast centers starting from 2019.

ACKNOWLEGEMENTS

This article/publication is based upon work from COST Action ES1303 'TOPROF' supported by COST (European Cooperation in Science and Technology, www.cost.eu).

REFERENCES

Baars, H. and Coauthors, 2016: An overview of the first decade of Polly^{NET}: an emerging network of automated Raman-polarization lidars for continuous aerosol profiling. *Atmos. Chem. Phys.*, **16**, 5111-5137. doi:10.5194/acp-16-5111-2016.

Benedetti, A. and Coauthors, 2009: Aerosol analysis and forecast in the European Centre for Medium-Range Weather Forecasts Integrated Forecast System: 2. Data assimilation. *J. Geophys. Res.,* **141** D13205. doi:10.1029/2008JD011115.

Cadeddu, M. P., Liljegren, J. C., and Turner, D. D., 2013: The Atmospheric radiation measurement (ARM) program network of microwave radiometers: instrumentation, data, and retrievals. *Atmos. Meas. Tech*., **6**, 2359–2372, https://doi.org/10.5194/amt-6- 2359-2013.

491 Caumont O., D., and Coauthors 2016: Assimilation of humidity and temperature observations
492 retrieved from ground-based microwave radiometers into a convective-scale model. *Q. J. R.*
493 *Meteorol. Soc.*, **142**: 2692–2704. doi:10.1002/qj.2860.

494 Cazorla, A., and Coauthors, 2017: Near-real-time processing of a ceilometer network assisted
495 with sun-photometer data: monitoring a dust outbreak over the Iberian Peninsula. *Atmos.*
496 *Chem. Phys*., **17**, 11861–11876. https://doi.org/10.5194/acp-17-11861-2017.

497 Chan, K. L., and Coauthors, 2018: Evaluation of ECMWF-IFS (version 41R1) operational
498 model forecasts of aerosol transport by using ceilometer network measurements. *Geosci.*
499 *Model. Dev.*, **11**, 3807-3831. doi.org/10.5194/gmd-11-3807-2018.

500 Cimini, D., M. Nelson, J. Güldner, and R. Ware, 2015: Forecast indices from a ground-based
501 microwave radiometer for operational meteorology. *Atmos. Meas. Tech*., **8**, 315-333,
502 https://doi.org/10.5194/amt-8-315-2015.
503 Cimini, D., and Coauthors, 2018: Uncertainty of atmospheric microwave absorption model:
504 impact on ground-based radiometer simulations and retrievals. *Atmos. Chem. Phys.*
505 *Discuss.*, https://doi.org/10.5194/acp-2018-536. In review.
506 De Angelis, F., and Coauthors, 2016: RTTOV-gb – adapting the fast radiative transfer model
507 RTTOV for the assimilation of ground-based microwave radiometer observations. *Geosci.*
508 *Model Dev*., **9**, 2721–2739, https://doi.org/10.5194/gmd-9-2721-2016.
509 De Angelis, F., and Coauthors, 2017: Long-term observations minus background monitoring
510 of ground-based brightness temperatures from a microwave radiometer network. *Atmos.*
511 *Meas. Tech.*, **10**, 3947-3961, https://doi.org/10.5194/amt-10-3947-2017.
512 Fernald, F. G., B. M. Herman, and J. A. Reagan, 1972: Determination of Aerosol Height
513 Distributions by Lidar, *J. Appl. Meteorol.*, **11,** 482–489, doi:10.1175/1520-
514 0450(1972)011<0482:DOAHDB>2.0.CO;2.

515 Gryning, S.E., and Coauthors, 2016: Weibull wind-speed distribution parameters derived from
516 a combination of wind-lidar and tall-mast measurements over land, coastal and marine sites.
517 *Boundary-Layer Meteorol*., **159**, 329–348, doi:10.1007/s10546-015-0113-x.
518 Haeffelin, M., and Coauthors, 2012: Evaluation of mixing height retrievals from automatic
519 profiling lidars and ceilometers in view of future integrated networks in Europe. *Boundary-*
520 *Layer Meteorol.,* **143**, 49–75.
521 Haeffelin, M., and Coauthors, 2016: Radiation fog formation alerts using attenuated
522 backscatter power from automatic Lidars and ceilometers. *Atmos. Meas. Tech*., **9**, 5347-
523 5365.
524 Hervo, M., Y. Poltera, and A. Haefele, 2016: An empirical method to correct for temperature-
525 dependent variations in the overlap function of CHM15k ceilometers. *Atmos. Meas. Tech.*,
526 **9**, 2947–2959, doi:10.5194/amt-9-2947-2016.
527 Hopkin, E, and Coauthors, 2018: A robust automated technique for operational calibration of
528 ceilometers using the integrated backscatter from totally attenuating liquid clouds.
529 Submitted to *Atmos. Meas. Tech.*
530 Illingworth, A. J., and Coauthors, 2007: Cloudnet: Continuous evaluation of cloud profiles in
531 seven operational models using ground-based observations. *Bull. Amer. Meteor. Soc.*, **88**,
532 883–898, doi:10.1175/BAMS-88-6-883.
533 Illingworth, A. J., and Coauthors, 2015: Exploiting Existing Ground-Based Remote Sensing
534 Networks to Improve High-Resolution Weather Forecasts. *Bull. Amer. Meteor. Soc.*, **96**,
535 2107-2125, doi:10.1175/BAMS-D-13-00283.1
536 Klett, J. D., 1985: Lidar Inversion with Variable Backscatter Extinction Ratios. *Appl. Opt*., **24**,
537 1638–1643, doi: 10.1364/AO.24.001638.

538 Kotthaus, S. and C. S. B. Grimmond, 2018: Atmospheric Boundary Layer Characteristics from
539 Ceilometer measurements Part 1: A new method to track mixed layer height and classify
540 clouds. *Q. J. R. Meteorol. Soc.*, in press, doi:10.1002/qj.3299.
541 Kotthaus, S., and Coauthors, 2016: Recommendations for processing atmospheric attenuated
542 backscatter profiles from Vaisala CL31 ceilometers. *Atmos. Meas. Tech.*, **9**, 3769–3791,
543 doi:10.5194/amt-9-3769-2016.
544 Lotteraner, C., and M. Piringer, 2016: Mixing-height time series from operational ceilometer aerosol-
545 layer heights. *Boundary-Layer Meteorology*, **161**, 265-287
546 Manninen A. J., O'Connor, E. J., Vakkari, V. and T. Petäjä, 2016: A generalised background
547 correction algorithm for a Halo Doppler lidar and its application to data from Finland.
548 *Atmos. Meas. Tech.*, **9**, 817–827, doi:10.5194/amt-9-817-2016.
549 Manninen A. J., T. Marke, M. Tuononen, and E. J. O'Connor, 2018: Atmospheric boundary
550 layer classification with Doppler lidar. *J. Geophys. Res*., Accepted for publication.
551 doi: 10.1029/2017jd028169.
552 Marke, T., and Coauthors, 2018: Long-Term Observations and High-Resolution Modeling of
553 Midlatitude Nocturnal Boundary Layer Processes Connected to Low-Level Jets. *J. Appl.*
554 *Meteor. Climatol.*, **57**, 1155–1170, https://doi.org/10.1175/JAMC-D-17-0341.1.
555 Martinet, P., D. and Coauthors, 2017: Combining ground-based microwave radiometer and the
556 AROME convective scale model through 1DVAR retrievals in complex terrain: an Alpine
557 valley case study. *Atmos. Meas. Tech.*, **10**, 3385-3402. https://doi.org/10.5194/amt-10-
558 3385-2017.
559 O'Connor, E. J., A. J. Illingworth, and R. J. Hogan, 2004: A technique for autocalibration of
560 cloud lidar. *J. Atmos. Ocean. Technol*., **21**, 777–786.

EJ O'Connor, E.J. and Coauthors, 2010: A method for estimating the turbulent kinetic energy dissipation rate from a vertically-pointing Doppler lidar, and independent evaluation from balloon-borne in-situ measurements. *J. Ocean and Atmos Tech.,* **27**, 1652-1664.

Päschke, E., R. Leinweber, and V. Lehmann, 2015: An assessment of the performance of a 1.5 µm Doppler lidar for operational vertical wind profiling based on a 1-year trial. *Atmos. Meas. Tech.*, **8**, 2251-2266. https://doi.org/10.5194/amt-8-2251-2015.

Pattantyús-Ábrahám, M., and Coauthors, 2017: The Dataset of the CeiLinEx 2015 Ceilometer-Inter-comparison Experiment, Version v001, doi 10.5676/DWD/CEILINEX2015.

Poltera, Y., and Coauthors, 2017: Pathfinder TURB: an automatic boundary layer algorithm. Development, validation and application to study the impact on in-situ measurements at the Jungfraujoch. *Atmos. Chem. Phys*., **17**, 10051-10070. https://doi.org/10.5194/acp-17-10051-2017.

Román, R., and Coauthors, 2018: Retrieval of aerosol profiles combining sun-photometer and ceilometer measurements in GRASP code. *Atmospheric Research*, **204**, 161-177.

Rottner, L., C. Baehr, A. Dabas and L. Hammoud, 2017: Stochastic method for turbulence estimation from Doppler lidar measurements. *Journal of Applied Remote Sensing* **11**(4), 046001. doi:10.1117/1.JRS.11.046001.

Rose, T., S. Crewell, U. Löhnert, and C. Simmer, 2005: A network suitable microwave radiometer for operational monitoring of the cloudy atmosphere. *Atmos. Res.*, **75**, 183–200, https://doi.org/10.1016/j.atmosres.2004.12.005.

Seity, Y., and Coauthors, 2011: The AROME-France convective- scale operational model, *Mon. Weather Rev.*, **139**, 976–991.

Schween, J. H., A. Hirsikko, U. Löhnert, and S. Crewell, 2014: Mixing layer height retrieval with ceilometer and Doppler lidar: from case studies to long-term assessment. *Atmos. Meas. Tech.*, **7,** 3685-3704. http://dx.doi.org/10.5194/amt-7-3685-2014.

586 Suomi, I., S.-E. Gryning, E. J. O'Connor, and T. Vihma, 2017: Methodology for obtaining wind
587 gusts using Doppler lidar. *Q.J.R. Meteorol. Soc.*, **143**: 2061–2072. doi:10.1002/qj.3059.
588 Teschke, G. and V. Lehmann, 2017: Mean wind vector estimation using the velocity–azimuth
589 display (VAD) method: an explicit algebraic solution. *Atmos. Meas. Tech*., **10**, 3265-3271.
590 https://doi.org/10.5194/amt-10-3265-2017.
591 Tuononen, M., E.J. O'Connor, V.A. Sinclair, and V. Vakkari, 2017: Low-Level Jets over Utö,
592 Finland, Based on Doppler Lidar Observations. *J. Appl. Meteor. Climatol*., **56**, 2577–2594.
593 https://doi.org/10.1175/JAMC-D-16-0411.1.
594 Vakkari, V., E. J. O'Connor, A. Nisantzi, R. E. Mamouri, and D. G. Hadjimitsis, 2015: Low-
595 level mixing height detection in coastal locations with a scanning Doppler lidar. *Atmos.*
596 *Meas. Tech.*, **8**, 1875-1885. doi:10.5194/amt-8-1875-2015.
597 Ware, R., and Coauthors, 2003: A multichannel radiometric profiler of temperature,
598 humidity, and cloud liquid. *Radio Sci*., **38**, 8079, https://doi.org/10.1029/2002RS002856,
599 2003.
600 Warren, E., and Coauthors, 2018: Evaluation of forward-modelled attenuated backscatter
601 using an urban ceilometer network in London under clear-sky conditions. *Atmos. Environ*.,
602 **191,** 532-547. doi:https://doi.org/10.1016/j.atmosenv.2018.04.045.
603 Westbrook, C. D., A. J. Illingworth, E. J. O'Connor, and R. J. Hogan, 2010: Doppler lidar
604 measurements of oriented planar ice crystals falling from supercooled and glaciated cloud
605 layers. *Q. J. R. Meteorol. Soc*., **136**, 260–276. doi:10.1002/qj.528.
606 Wiegner, M. and A. Geiß, 2012: Aerosol profiling with the Jenoptik ceilometer CHM15kx.
607 *Atmos. Meas. Tech.*, **5**, 1953–1964. doi:10.5194/amt-5-1953-2012.
608 Wiegner, M., and Coauthors, 2014: What is the benefit of ceilometers for aerosol remote
609 sensing? An answer from EARLINET. *Atmos. Meas. Tech.*, **7**, 1979-1997,
610 https://doi.org/10.5194/amt-7-1979-2014.

Wiegner, M and J. Gasteiger. 2015: Correction of water vapor absorption for aerosol remote sensing with ceilometers. *Atmos. Meas. Tech.*, **8,** 3971–3984. doi:10.5194/amt-8-3971-2015.

SIDEBAR: THE TOPROF COST ACTION

COST or 'European Cooperation in Science and Technology' is a European Union funded program that enables researchers to set up an interdisciplinary research networks in Europe and beyond. Twenty-two European countries participated in the TOPROF action with researchers from 16 National Weather Services attending together with representatives from six European manufacturers of ALCs, DWLs and MWRs. Three day meetings were held twice a year each with about 50 participants, but most importantly TOPROF supported 24 separate week long visits by individual scientists to other research labs, national weather services, or industry, where they tackled specific problems such as: changes to calibration procedures, modifications to data processing that resulted in new public releases of software, physical modification of the instruments and testing of forward models at national weather services. In addition, there were 12 special meetings to plan, execute and discuss field projects dedicated to comparing the performance of different instruments with various configurations, and in some cases with independent validation using instrumented towers and/or special radiosonde ascents.

FIGURE CAPTIONS

Fig. 1. Map of the ALC network (green - operational E-PROFILE stations: blue - stations planned for 2018: red - other ceilometers reported by DWDs ceilomap). Example of E-PROFILE measurements during the Saddleworth Moor fire near Manchester (26 to 27 June 2018). Five stations are represented: Stornoway, Eskdalemuir, Flesland, Rotterdam and Ulrichstein. A photograph of the fire (courtesy E. J. O'Connor) is shown in the lower left corner.

Fig 2. The 1064 nm attenuated backscatter for a frontal passage over Ulm, Germany on 25 August 2018 measured by a CHM15k ceilometer. Clouds and rain appear in black, red and orange colors. Areas in green, yellow, and orange are aerosol layers. Areas above clouds where the ceilometer signal is extinguished are plotted in white.

Fig 3. ALC measurements from eight co-located ALCs including Campbell Scientific, Vaisala, and Lufft instruments based on 3 hours of data on 13 Aug 2015 during the Ceilinex campaign in Lindenberg, Germany. (Left panel) raw instrument signal; (Right panel) calibrated attenuated backscatter signal. 1 Mm = 10^6 m. Note the increased noise for the CL31 above 2km and the divergence of the profiles below 500 m.

Fig. 4. Upper left panel: Attenuated Backscatter measured by the CHM15k in Valladolid during a Saharan dust event from 20 to 27 June 2018. Data above clouds and with SNR lower than 3 are removed. Lower left panel: Attenuated Backscatter forecast by CAMS model at the closest grid point. Upper right panel: Median attenuated backscatter measured (in red) and forecast (in black). Lower right panel: median of the bias between observations and forecasts. Shading represents 25^{th} and 75^{th} percentiles.

Fig. 5. Three-hour time series plot generated automatically from measurements taken at Charles-de-Gaulle airport (France) on 21 Jan 2016. (Top panel): fog alerts based on the method of Haeffelin et al. (2016). (Lower panel): 0-400m ALC attenuated backscatter profile (m^{-1} sr^{-1}, shown on a colored log scale) and horizontal visibility close to the surface (m, shown as a gray line, the vertical axis shows the visibility on a log scale). The 1-km horizontal-visibility

threshold, adopted by WMO to define fog, is shown as a gray dashed line. Plots generated in real-time are available at: http://www.lmd.polytechnique.fr/~sirta/parafog/.

Fig. 6. 24-hour time-height plots of Doppler lidar products generated from a Halo Photonics Streamline operating in Helsinki, Finland, on 24 March 2014: (a) attenuated backscatter coefficient, (b) wind speed including objective low-level jet diagnosis (black circles), (c) wind direction, (d) dissipation rate of turbulent kinetic energy. The wind profiles are obtained from scans at two elevations, 15 and 70 degrees from horizontal. Helsinki is situated on a coast line that is aligned approximately east-west and the Doppler lidar is located about 6 km inland from the coast. This combination of products illustrates the complexity of the boundary layer in a coastal and urban environment, with a sea breeze driving a marine boundary layer inland (northerly low-level flow from sea to land) underneath a much deeper land boundary layer (more southerly flow from land to sea aloft). Solar noon is around 10 UTC, and after 1900 UTC all flow is from land to sea.

Fig. 7. One-year time series of the O–B T_B differences at Jülich (adapted from De Angelis et al. 2017). From top to bottom: channels 22.24 (blue), 31.40 (red), 52.28 (magenta), and 58.00 GHz (cyan). Typically, RMS at zenith are within 3 K with low bias; for instrument, channel, and observing angle dependencies see De Angelis et al. (2017). The black circle indicates the date of a new liquid nitrogen calibration. Were such a monitoring available operationally, the faulty calibration could have been detected earlier and the recalibration could have been validated in near-real-time. The NWP model used here is AROME, Application of Research to Operations at Mesoscale, developed by Météo-France (Seity et al., 2011).

Fig. 8. Profiles of RMSE with respect to radiosonde observations of the AROME NWP model

686 background (dashed) and 1DVAR updated analysis (solid) in clear (left) and cloudy (right) sky
687 conditions. During stable conditions in an enclosed alpine valley, 1DVAR assimilation of
688 MWR brightness temperatures lead to an improvement in the temperature analysis in the first
689 1500 m up to 7.5 K in clear conditions and up to ~4 K in cloudy conditions. Data from the
690 Passy-2015 field campaign (December 2014 to March 2015), Arve River valley near Passy,
691 France (Martinet et al., 2017).
692
693 **Fig. 9.** 24-hour time series (28 October 2016) of temperature (top) and humidity (bottom) from
694 AROME NWP model (left), 1DVAR analysis update (center), and the difference between the
695 two (right) showing temperature increments of up to 5 K. Data from a fog field campaign at
696 Observatoire Perenne de l'Environnement (Lat: 48.56; Lon: 5.50; Alt: 388 m) near Bure
697 (France). The campaign extended from Sep 2015 to Apr 2016 and included one MWR unit.
698 NWP system is AROME 1h forecast cycle, 1.3 km horizontal resolution, 90 vertical levels.
699 The nearest grid-point 1-hour forecast is used as background for the 1DVAR retrievals at 1-
700 hour resolution, based on the closest measurements within 15 minutes.
701
702
703
704

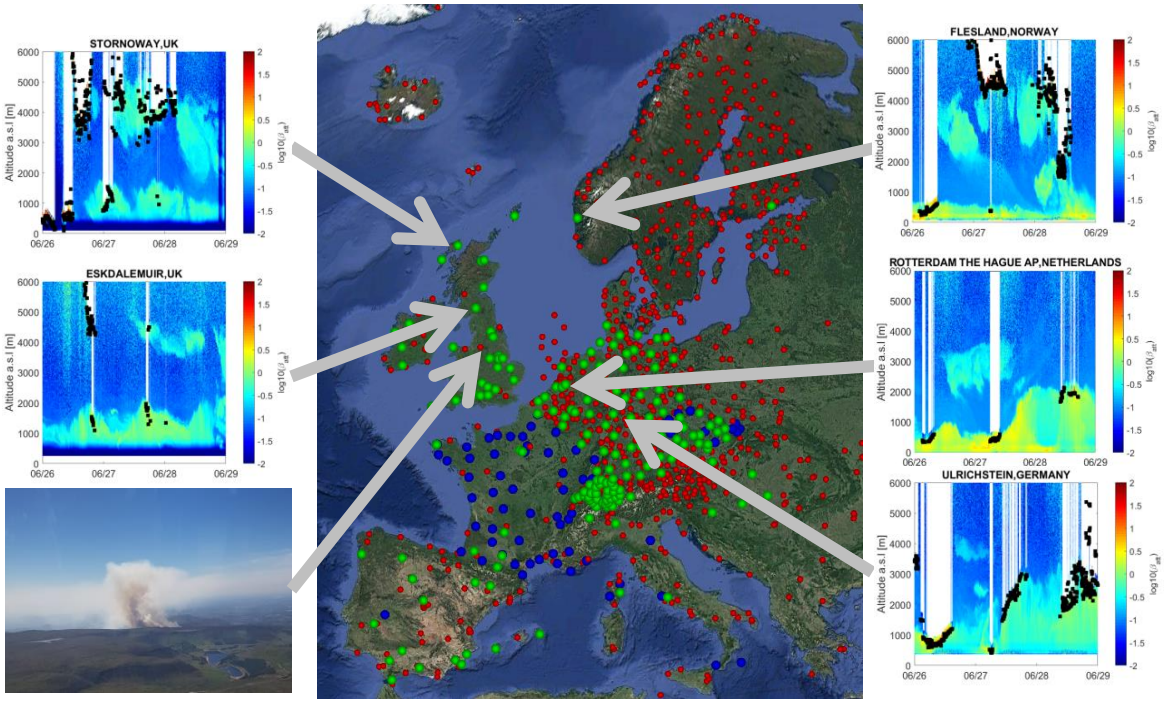

705
706

707 **Fig. 1.** Map of the ALC network (green - operational E-PROFILE stations: blue - stations
708 planned for 2018: red - other ceilometers reported by DWDs ceilomap). Example of E-
709 PROFILE measurements during the Saddleworth Moor fire near Manchester (26 to 27 June
710 2018). Five stations are represented: Stornoway, Eskdalemuir, Flesland, Rotterdam and
711 Ulrichstein. A photograph of the fire (courtesy E. J. O'Connor) is shown in the lower left
712 corner.

713
714
715
716
717
718
719

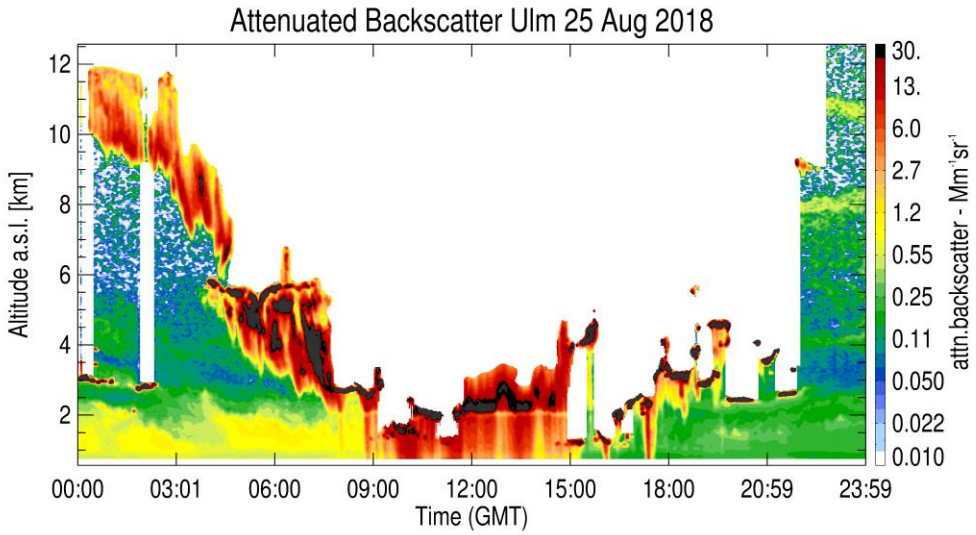

720

721

722 **Fig 2.** The 1064 nm attenuated backscatter for a frontal passage over Ulm, Germany on 25
723 August 2018 measured by a CHM15k ceilometer. Clouds and rain appear in black, red and
724 orange colors. Areas in green, yellow, and orange are aerosol layers. Areas above clouds where
725 the ceilometer signal is extinguished are plotted in white.

726

727

728

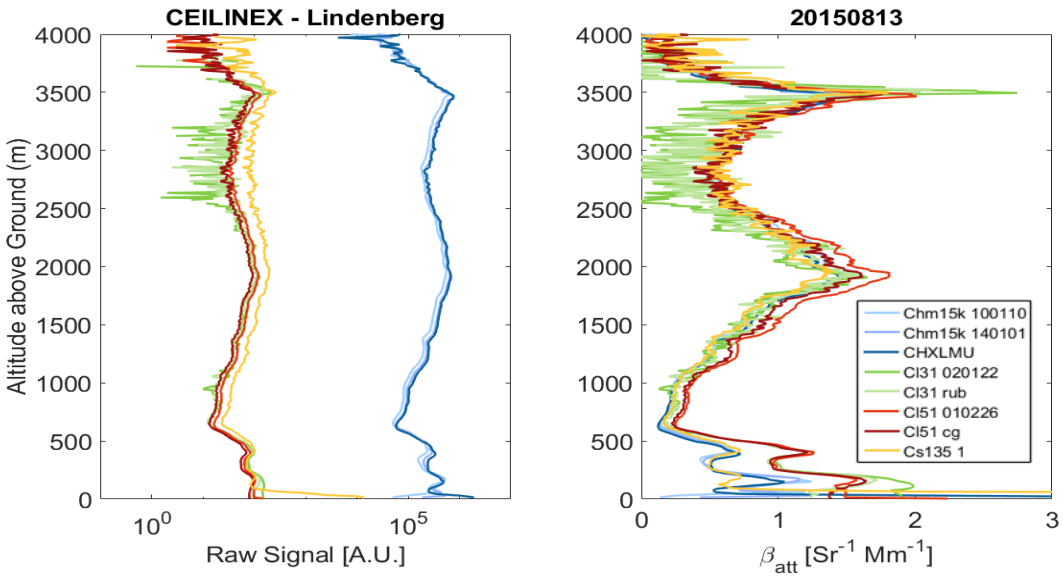

729

730

731 **Fig. 3** ALC measurements from eight co-located ALCs including Campbell Scientific, Vaisala,
732 and Lufft instruments based on 3 hours of data on 13 Aug 2015 during the Ceilinex campaign
733 in Lindenberg, Germany. (Left panel) raw instrument signal; (Right panel) calibrated
734 attenuated backscatter signal. 1 Mm = 10^6 m. Note the increased noise for the CL31 above 2km
735 and the divergence of the profiles below 500 m.

736

737

738

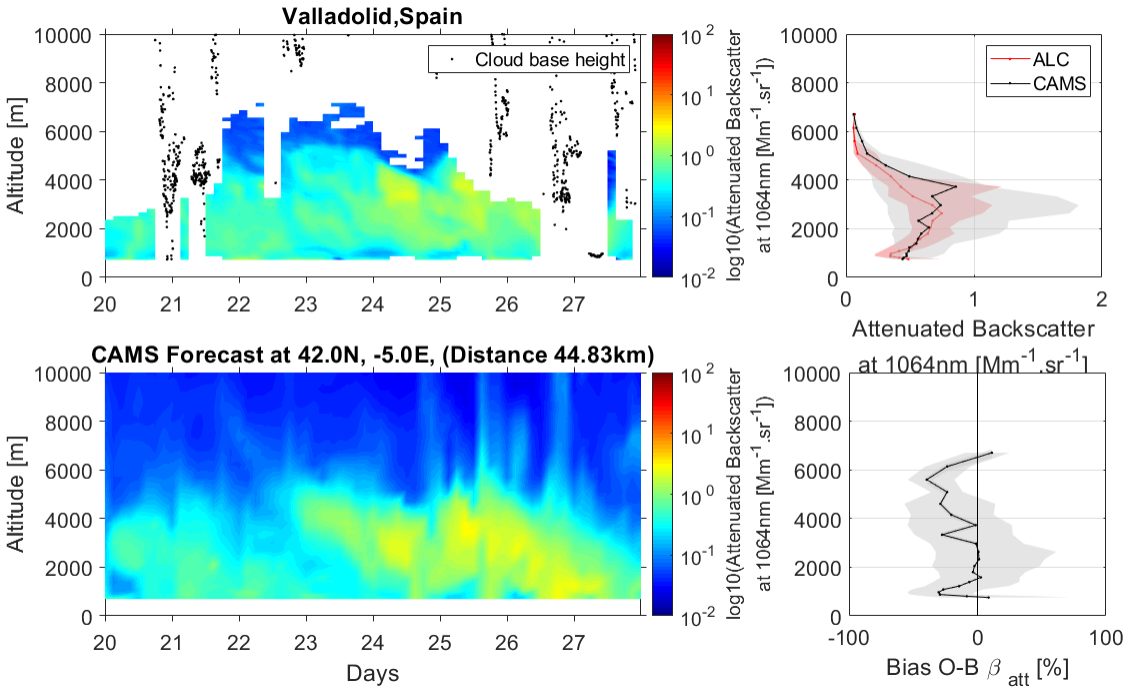

739
740
741

742 **Fig. 4**. Upper left panel: Attenuated Backscatter measured by the CHM15k in Valladolid
743 during a Saharan dust event from 20 to 27 June 2018. Data above clouds and with SNR lower
744 than 3 are removed. Lower left panel: Attenuated Backscatter forecast by CAMS model at the
745 closest grid point. Upper right panel: Median attenuated backscatter measured (in red) and
746 forecast (in black). Lower right panel: median of the bias between observations and forecasts.
747 Shading represents 25th and 75th percentiles

748
749
750
751

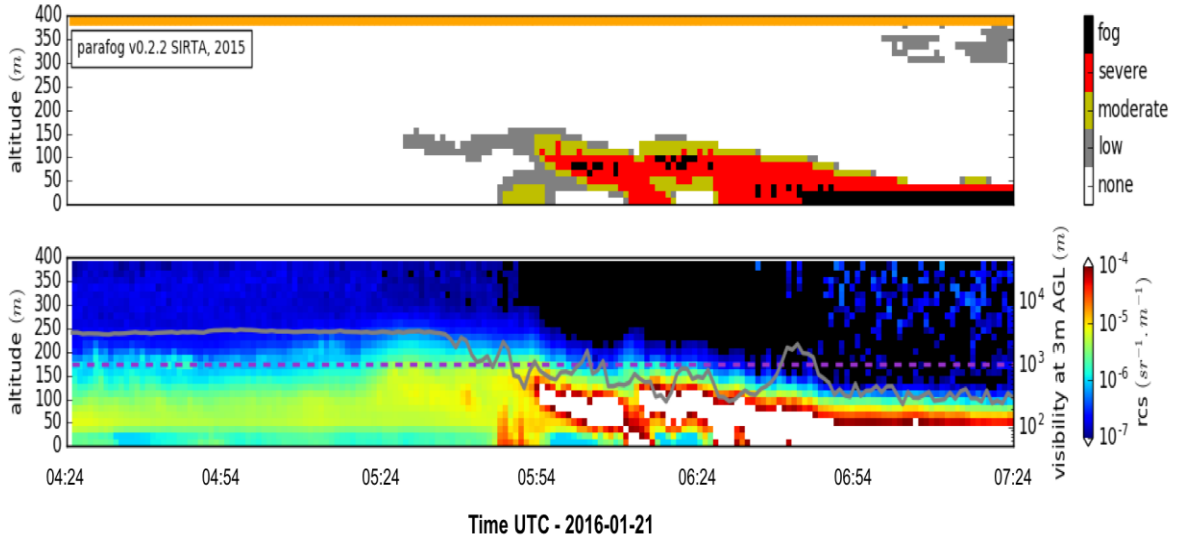

752

753

754 **Fig. 5**. Three-hour time series plot generated automatically from measurements taken at
755 Charles-de-Gaulle airport (France) on 21 Jan 2016. (Top panel): fog alerts based on the method
756 of Haeffelin et al. (2016). (Lower panel): 0-400 m ALC attenuated backscatter profile (m^{-1} sr^{-1},
757 shown on a colored log scale) and horizontal visibility close to the surface (m, shown as a
758 gray line, the vertical axis shows the visibility on a log scale). The 1-km horizontal-visibility
759 threshold, adopted by WMO to define fog, is shown as a gray dashed line. Plots generated in
760 real-time are available at: http://www.lmd.polytechnique.fr/~sirta/parafog/.

761

762

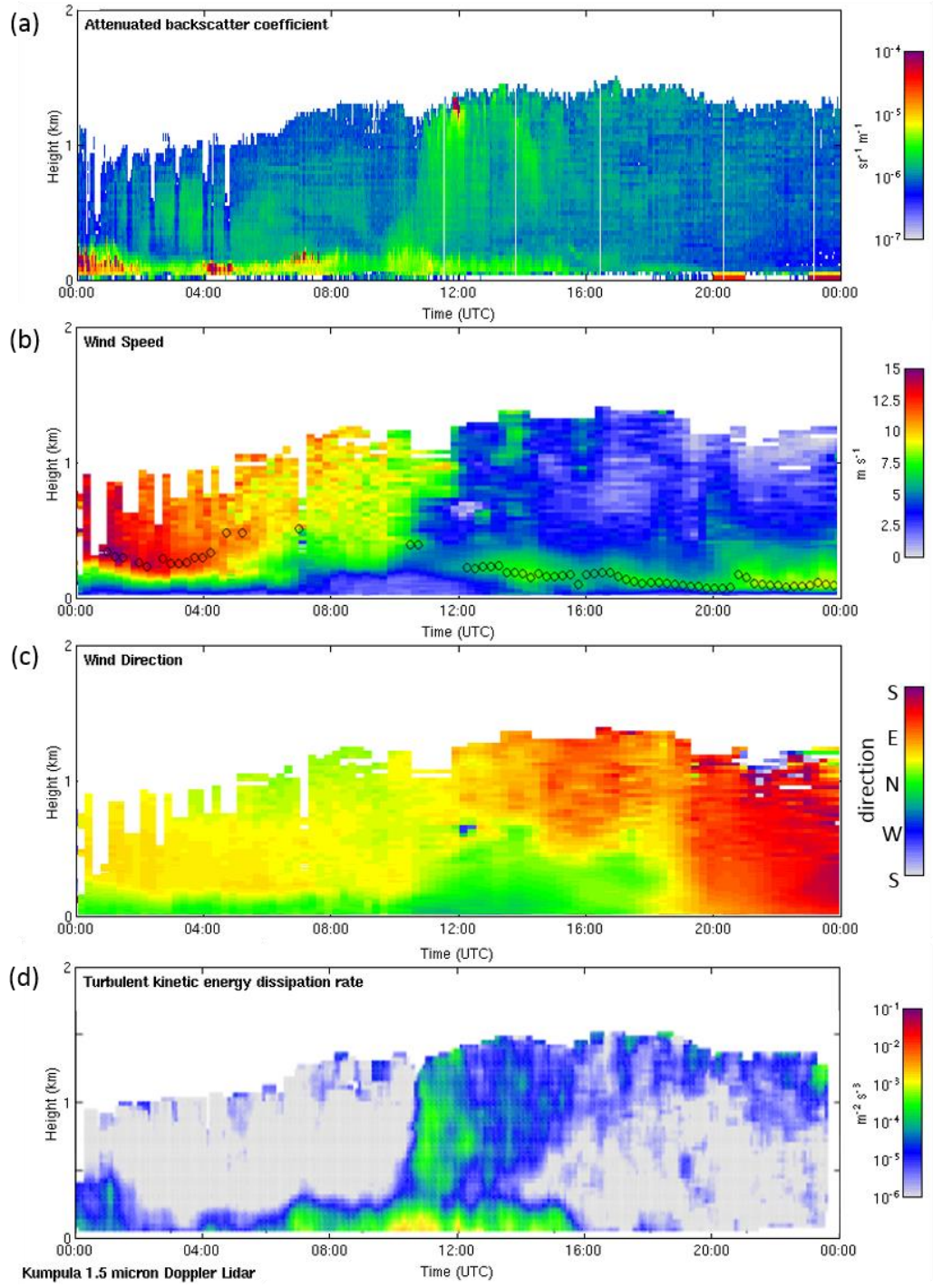

Fig. 6. 24-hour time-height plots of Doppler lidar products generated from a Halo Photonics Streamline operating in Helsinki, Finland, on 24 March 2014: (a) attenuated backscatter coefficient, (b) wind speed including objective low level jet diagnosis (black circles), (c) wind direction, (d) dissipation rate of turbulent kinetic energy. The wind profiles are obtained from scans at two elevations, 15 and 70 degrees from horizontal. Helsinki is situated on a coast line

that is aligned approximately east-west and the Doppler lidar is located about 6 km inland from the coast. This combination of products illustrates the complexity of the boundary layer in a coastal and urban environment, with a sea breeze driving a marine boundary layer inland (northerly low-level flow from sea to land) underneath a much deeper land boundary layer (more southerly flow from land to sea aloft). Solar noon is around 10 UTC, and after 1900 UTC all flow is from land to sea.

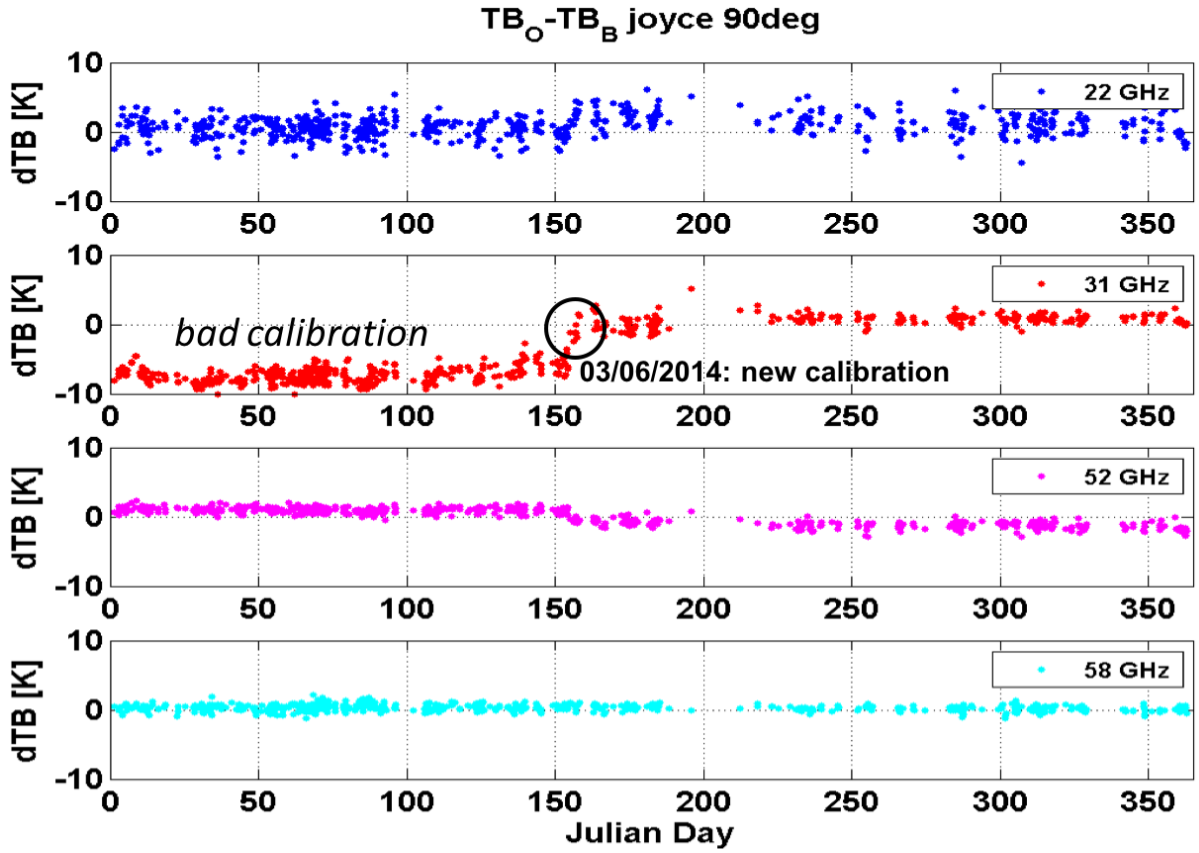

Fig. 7. One-year time series of the O–B T_B differences at Jülich (adapted from De Angelis et al. 2017). From top to bottom: channels 22.24 (blue), 31.40 (red), 52.28 (magenta), and 58.00 GHz (cyan). Typically, RMS at zenith are within 3 K with low bias; for instrument, channel, and observing angle dependencies see De Angelis et al. (2017). The black circle indicates the date of a new liquid nitrogen calibration. Were such a monitoring available operationally, the faulty calibration could have been detected earlier and the recalibration could have been

validated in near-real-time. The NWP model used here is AROME, Application of Research to Operations at Mesoscale, developed by Météo-France (Seity et al., 2011).

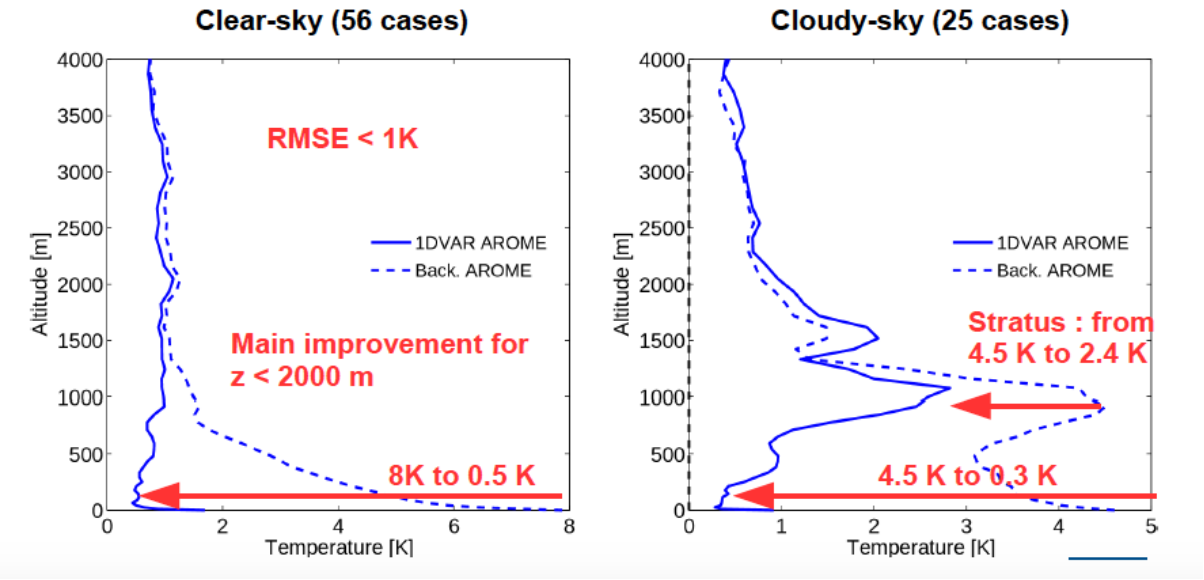

Fig. 8. Profiles of RMSE with respect to radiosonde observations of the AROME NWP model background (dashed) and 1DVAR updated analysis (solid) in clear (left) and cloudy (right) sky conditions. During stable conditions in an enclosed alpine valley, 1DVAR assimilation of MWR brightness temperatures lead to an improvement in the temperature analysis in the first 1500 m up to 7.5 K in clear conditions and up to ~4 K in cloudy conditions. Data from the Passy-2015 field campaign (December 2014 to March 2015), Arve River valley near Passy, France (Martinet et al., 2017).

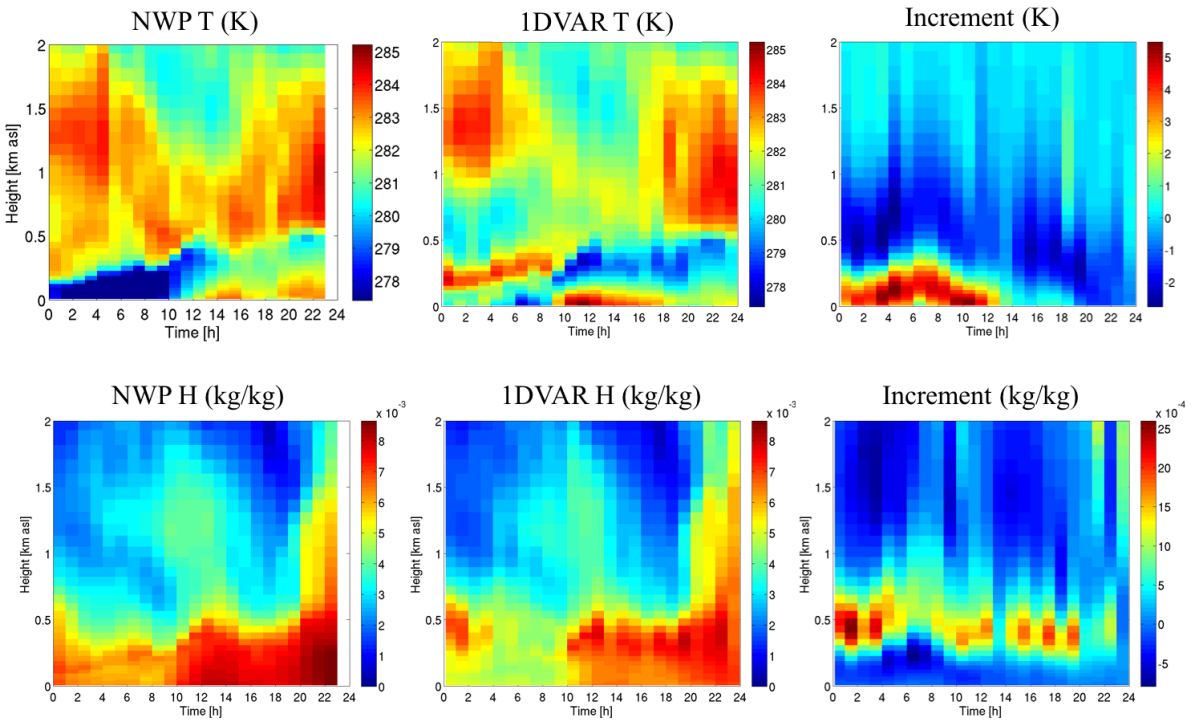

Fig. 9. 24-hour time series (28 October 2016) of temperature (top) and humidity (bottom) from AROME NWP model (left), 1DVAR analysis update (center), and the difference between the two (right) showing temperature increments of up to 5 K. Data from a fog field campaign at Observatoire Perenne de l'Environnement (Lat: 48.56; Lon: 5.50; Alt: 388 m) near Bure (France). The campaign extended from Sep 2015 to Apr 2016 and included one MWR unit. NWP system is AROME 1h forecast cycle, 1.3 km horizontal resolution, 90 vertical levels. The nearest grid-point 1-hour forecast is used as background for the 1DVAR retrievals at 1-hour resolution, based on the closest measurements within 15 minutes.